JBC RESEARCH ARTICLE

SENP3 mediates the deSUMOylation and degradation of YAP1 to regulate the progression of triple-negative breast cancer

Received for publication, March 17, 2024, and in revised form, July 23, 2024 Published, Papers in Press, September 11, 2024,
https://doi.org/10.1016/j.jbc.2024.107764

Xu Chen[1,†], Danqing Li[1,†], Qi Su[1,†], Xing Ling[1], Yanyan Yang[1], Yuhang Liu[1], Xinjie Zhu[1], Anqi He[1], Siyu Ding[1], Runxiao Xu[1], Zhaoxia Liu[1], Xiaojun Long[1], Jinping Zhang[2], Zhihui Yang[2], Yitao Qi[1,*], and Hongmei Wu[1,*]

From the [1]College of Life Sciences, Shaanxi Normal University, Xi'an, Shaanxi, China; [2]Department of Pathology, The Affiliated Hospital of Southwest Medical University, Luzhou, Sichuan, China

Reviewed by members of the JBC Editorial Board. Edited by Paul Shapiro

Triple-negative breast cancer (TNBC) is a prevalent malignancy in women, casting a formidable shadow on their well-being. Positioned within the nucleolus, SUMO-specific protease 3 (SENP3) assumes a pivotal role in the realms of development and tumorigenesis. However, the participation of SENP3 in TNBC remains a mystery. Here, we elucidate that SENP3 exerts inhibitory effects on migration and invasion capacities, as well as on the stem cell–like phenotype, within TNBC cells. Further experiments showed that YAP1 is the downstream target of SENP3, and SENP3 regulates tumorigenesis in a YAP1-dependent manner. YAP1 is found to be SUMOylated and SENP3 deconjugates SUMOylated YAP1 and promotes degradation mediated by the ubiquitin-proteasome system. More importantly, YAP1 with a mutation at the SUMOylation site impedes the capacity of WT YAP1 in TNBC tumorigenesis. Taken together, our findings firmly establish the pivotal role of SENP3 in the modulation of YAP1 deSUMOylation, unveiling novel mechanistic insight into the important role of SENP3 in the regulation of TNBC tumorigenesis in a YAP1-dependent manner.

Breast carcinoma presents a formidable public health conundrum, characterized by a considerable mortality rate (1–3). Remarkably, triple-negative breast cancer (TNBC), marked by its lack of estrogen receptor, progesterone receptor, and human epidermal growth factor 2 receptor expression, manifests inherent aggressiveness, accompanied by a bleak prognostic outlook (4–6). This variant encompasses 15 to 26% of the entire population of breast cancer patients (7–9). The increased propensity of TNBC to metastasize to healthy organs and its higher recurrence rate further contribute to its elevated mortality and unfavorable prognosis, making it the most malignant breast cancer subtype (10–12). Currently, the therapeutic approach to TNBC is based primarily on surgical interventions, chemotherapy regimens, and radiation therapy protocols. However, the absence of estrogen receptor, progesterone receptor, and human epidermal growth factor 2 receptor poses a formidable challenge in the application of conventional cancer treatments to patients with TNBC with optimal efficacy. Therefore, identifying the optimal treatment approach for patients with TNBC is particularly urgent.

SUMOylation stands as an example of the highly dynamic realm of posttranslational modifications, wherein the SUMO protein becomes intricately bound, covalently, or noncovalently, to the lysine residue of substrate proteins through a meticulously orchestrated enzyme cascade reaction (13–15). Orchestration of this cascade reaction requires a sequential interaction involving the activating enzyme E1, the binding enzyme E2, and the ligating enzyme E3. SUMOylation is a process susceptible to reversal by the illustrious family of SUMO-specific proteases (SENPs), within which mammals boast the expression of an impressive array comprising six distinct SENPs, namely SENP 1 to 3 and SENP 5 to 7 (16, 17). SENP3 is localized in the nucleolus and is an oxidative stress molecule (18). Mild oxidative stress exerts a fortifying influence on the stability of SENP3, facilitating its migration from the nucleolus to the nucleoplasm and effectively nullifying the SUMOylation activity of the target protein (19). SENP3 has been reported to regulate autophagy in mouse liver tissue (20–22). SENP3 is closely related to a variety of tumors, and oxidative stress-induced accumulation of SENP3 can enhance STAT3 activity and its carcinogenic function (23). Previous studies showed contradictory roles of SENP3 in breast cancer (24, 25), making further investigation necessary.

The Hippo signaling pathway, noted for its remarkable conservation in various organs and tissues, assumes a central role in the precise orchestration of organ and tissue dimensions, which deftly regulates both cell death mechanisms and the stimulation of cell proliferation (26). The Hippo pathway comprises three key components, including the upstream regulatory elements Mer and NF2, the core components mainly represented by LATS1/2, MST1/2, and the downstream effector YAP. Within the context of a well-balanced cellular process, activated MST1/2 triggers phosphorylation and activation of LATS1/2, culminating in phosphorylation of YAP. Then it serves as a barrier to its

† These authors contributed equally to the work.
* For correspondence: Yitao Qi, qiyitao@snnu.edu.cn; Hongmei Wu, hq8479@snnu.edu.cn.

nuclear translocation, thus modulating its role (27). Emerging evidence shows the close association of the Hippo signaling pathway with the incidence and progression of TNBC. Ring finger protein (RNF) 187 assumes a negative regulatory role within the Hippo pathway, and inhibition of RNF187 expression produces a substantial reduction in the migratory and invasive capacities of TNBC cells (28). Similarly, bisphenol reduces the phosphorylation level of Lats, promoting YAP expression and thus improving TNBC cell migration (29). Furthermore, the Wnt/β-catenin and Hippo pathways are critical in tumorigenesis, and dual inhibition of Wnt and YAP expression represents a potential novel strategy for the treatment of TNBC (30). Various posttranslational modifications, including phosphorylation and ubiquitination, are key modulators governing YAP activation or subcellular localization, and dysregulation of YAP modification has been linked to cancers (31, 32). YAP is also reported to be SUMOylated; however, whether SUMOylation has any effect on TNBC remains largely unknown.

Our discoveries reveal the role of SENP3 as a tumor suppressor gene, by which it exerts an inhibitory influence on cell migration and epithelial-mesenchymal transition (EMT) in TNBC cells. Mechanically, we demonstrate that YAP1 is predominantly modified by SUMO1, which enhances its protein stability. Furthermore, SENP3 deconjugates the SUMOylation of YAP1 and promotes its ubiquitination and degradation, effectively retarding the onset and progression of TNBC. Our study provides compelling evidence for SENP3-regulated YAP1 SUMOylation in regulating TNBC pathogenesis. These findings offer valuable insights into the molecular mechanisms that govern the development of TNBC and the broader clinical implications and therapeutic potential of targeting the SENP3–YAP1 axis.

Results

SENP3 knockdown promotes the proliferation and invasion of TNBC cells

To reveal the clinical implications of SENP3 expression, we analyzed the SENP3 transcriptional level of cancer patients with the TIMER2.0 database. The results illustrated that SENP3 was specifically downregulated in breast cancer tissue in contrast to normal controls (Fig. S1*A*). Furthermore, data from breast cancer patients within the GEPIA2 database showed that overall survival, recurrence-free survival, and distant metastasis-free survival characterized by elevated expression of SENP3 were significantly higher than those characterized by low expression of SENP3, suggesting an inverse correlation between SENP3 levels and adverse clinical outcomes (Fig. 1, *A*–*C*). Subsequently, we analyzed the expression of SENP3 using cancerous and paracancerous tissues from patients with TNBC. The results revealed a significantly decreased expression of SENP3 within breast cancer tissues (Fig. 1*D*), indicating that SENP3 was downregulated in TNBC tissues. SENP3 expression in various TNBC cell lines were detected and the results showed decreased expression of SENP3 in TNBC cells compared to mammary epithelial cells (Fig. S1*B*). SENP3 knockdown was induced in BT-549 and MDA-MB-231 cells (Fig. S1, *C* and *D*), and 3-(4, 5-dimethylthiazol-2-yl)-2, 5-diphenyltetrazolium bromide (MTT) assays revealed a notable increase in the proliferation of MDA-MB-231 and BT-549 cells after SENP3 knockdown, in stark contrast to their control counterparts (Figs. 1*E* and S1*E*). Additionally, colony formation capacity was increased after SENP3 depletion in MDA-MB-231 and BT-549 cells (Figs. 1*F* and S1*F*). Sequential experiments involving scratch and transwell techniques also substantiated the fact that suppression of SENP3 amplified the mobility and invasive potential of TNBC cells (Figs. 1, *G* and *H*, and S1*G* and *H*). Furthermore, the assessment of unanchored growth ability was carried out through the implementation of the soft agar pelletizing assay, which revealed intensified pellet formation in MDA-MB-231 cells with SENP3 elimination (Fig. 1*I*). Cancer stem cells are one of the critical types of cancer cells and are driven by intracellular genes that regulate cell pluripotency, such as *NANOG*, *OCT4*, and *SOX2*, which can self-renew and differentiate into a variety of malignant cell types (33). Furthermore, SENP3 suppression led to increased mRNA expression of the pluripotency-associated genes *NANOG*, *OCT4*, and *SOX2* (Fig. 1*J*), along with a change in the expression of the EMT markers, characterized by decreased epithelial markers and increased mesenchymal markers (Fig. 1*K*). Collectively, these results indicated that SENP3 elimination accelerated the migration and invasion of TNBC cells.

SENP3 overexpression inhibits TNBC cell proliferation and invasion

Furthermore, we engineered MDA-MB-231 and BT-549 cell lines with SENP3 overexpression (Fig. S2, *A* and *B*), and the MTT assay showed that SENP3 overexpression inhibited TNBC cell growth activity (Fig. 2*A*). This overexpression also led to a marked reduction in colony formation capacity (Fig. 2*B*) and decreased cell migration rates compared to control cells (Fig. 2*C*). Transwell experiments also indicated that SENP3 overexpression inhibited TNBC cell migration and invasion (Fig. 2*D*). Cells with SENP3 overexpression exhibited a reduced pellet formation capacity on soft agar, indicating a decreased unanchored growth capacity (Fig. 2*E*). Analysis of stem cell marker expression revealed that SENP3 overexpression significantly decreased mRNA levels of *NANOG*, *OCT4*, and *SOX2* (Fig. 2*F*), with an increase in epithelial markers and a decrease in mesenchymal markers (Fig. 2*G*). Collectively, SENP3 overexpression inhibited the migration, invasion, and EMT process of TNBC cells.

YAP1 acts as a downstream effector in SENP3-regulated TNBC cells

Increasing evidence shows that the Hippo–YAP1 signaling pathway plays a critical role in the progression of TNBC (34, 35). To identify whether Hippo–YAP1 signaling has any effect on SENP3-regulated TNBC cells, we first examined YAP1 expression in various cell lines and observed increased expression of YAP1 in TNBC cells compared to mammary

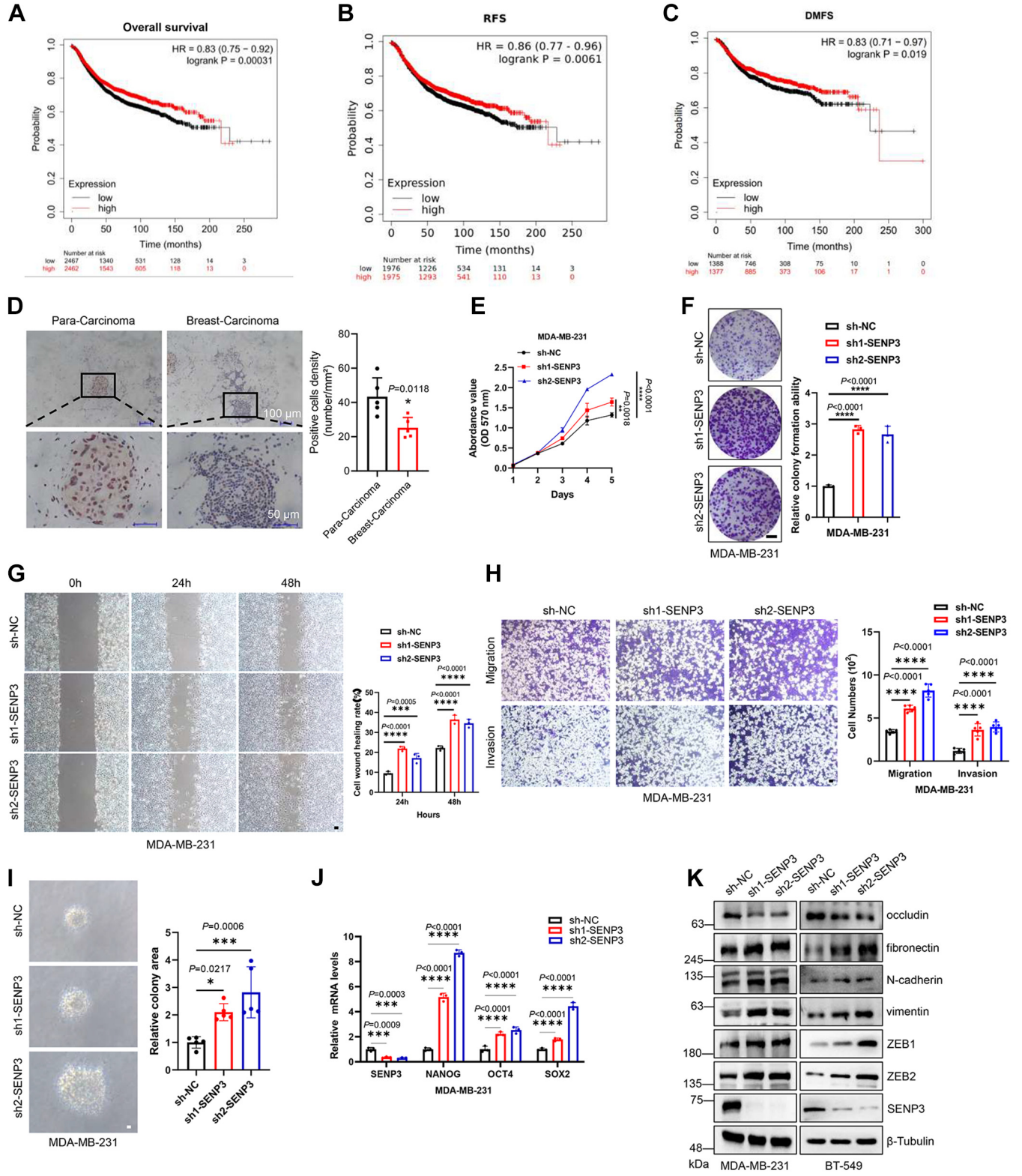

Figure 1. SENP3 knockdown promoted the proliferation and invasion of TNBC cells. *A–C*, SENP3 expression exhibited a favorable correlation with overall survival (*A*), recurrence-free survival (*B*), and distant metastasis-free survival (*C*) among breast cancer patients. SENP3 expression levels in breast cancer and normal tissue were examined using the GEPIA2 database. *D*, SENP3 was lowly expressed in TNBC patients. SENP3 level was analyzed and calculated in cancer and precancerous tissue from TNBC patients by immunohistochemistry with SENP3 antibody (n = 5). Hematoxylin (*blue*) was applied to visualize the nuclei. The scale bar represents 100 μm in *above panels* and 50 μm in *bottom panels*. *E*, SENP3 knockdown markedly increased the proliferation of MDA-MB-231 cells. Growth curves that define the progression of SENP3 knockdown and control cells were meticulously generated by daily quantification of cell numbers (n = 3 replicates/group). *F*, SENP3 knockdown promoted the colony formation of MDA-MB-231 cells. Cells were cultured in a 24-well plate for 2 weeks and stained with 0.1% crystal violet for the evaluation of colony formation (*left*). The evaluation of colony formation capacity was conducted (n = 3 replicates/group). The scale bar represents 200 μm. *G*, SENP3 knockdown significantly increased the migratory capacity of MDA-MB-231 cells. Cell migration was determined by a wound healing assay in stably transfected cells (*left*). The migration rate was calculated and analyzed (right, n = 3 repeats/

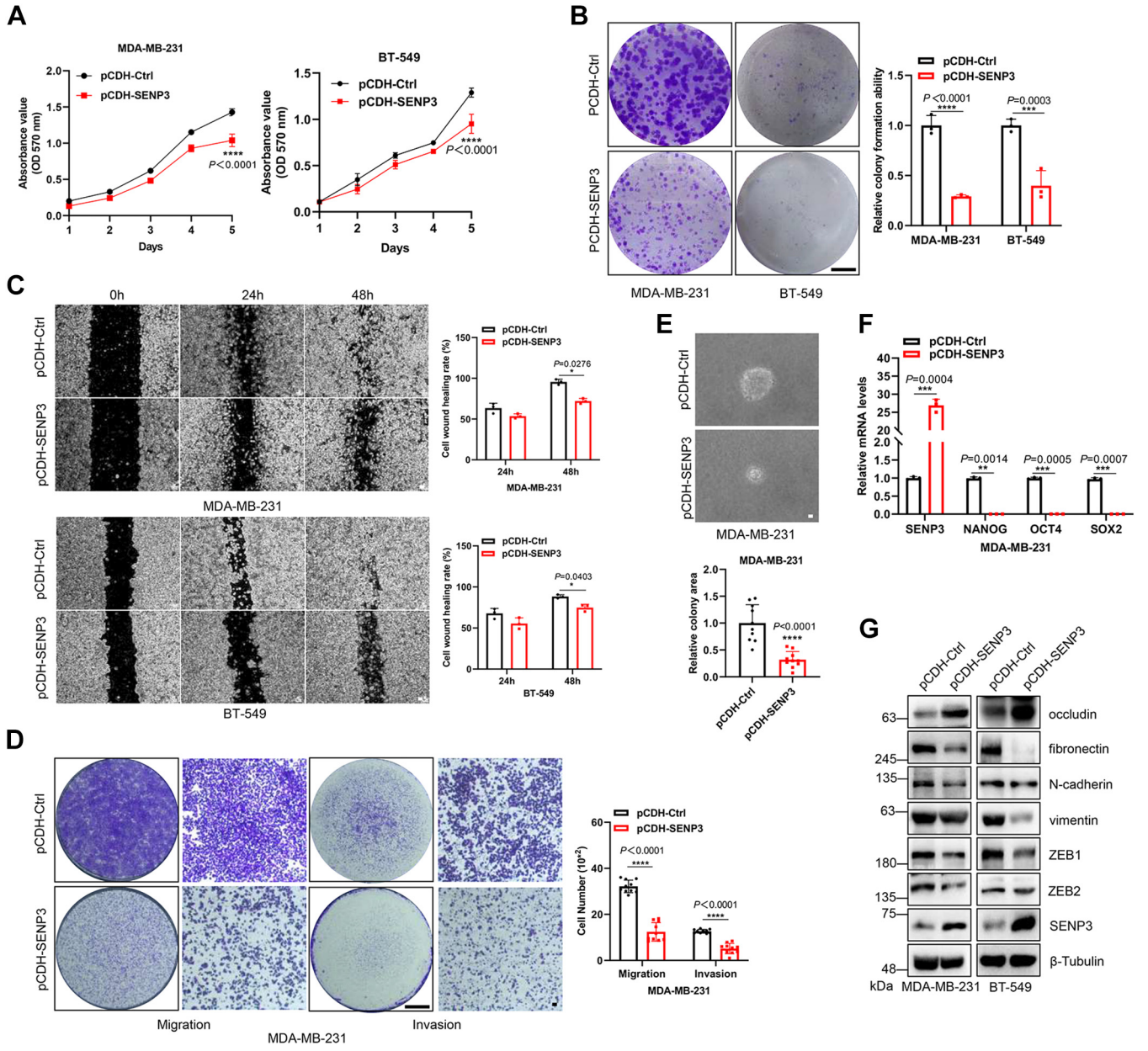

Figure 2. SENP3 overexpression inhibited the proliferation and invasion of TNBC cells. *A*, SENP3 overexpression conferred a suppressive effect on the proliferation of MDA-MB-231 and BT-549 cells. Growth curves representing SENP3 overexpression and control cells were generated by daily quantification of cell number (n = 3 repeats/group). *B*, SENP3 overexpression exhibited a suppressive effect on the colony formation of MDA-MB-231 and BT-549 cells. Cells were cultured in a 24-well plate for 2 weeks and stained with 0.1% crystal violet for the colony formation assay (*left*). The colony formation capacity was assessed (n = 3 repeats/group). The scale bar represents 200 μm. *C*, elevation of SENP3 expression caused a notable reduction in the migratory capacity of MDA-MB-231 and BT-549 cells. Cell migration was determined by a wound healing assay in stably transfected cells (*left*). Quantification and analysis of migration rates were carried out (*right*, n = 3 repeats/group). The scale bar represents 20 μm. *D*, SENP3 overexpression decreased MDA-MB-231 cell invasion. Evaluation of cell migration and invasion was conducted by transwell assay in stably transfected cells (*left*). The quantification and analysis of migratory and invasive cells was carried out (*right*, n = 10 repeats/group). The scale bar represents 200 μm (*left*) and 20 μm (*right*). *E*, SENP3 overexpression increased the unanchored growth of MDA-MB-231 cells. The formed *spheres* were observed and analyzed (*right*, n = 10 repeats/group). The scale bar represents 20 μm. *F*, SENP3 overexpression increased the transcription of stem cell markers in MDA-MB-231 cells. Gene transcript expression levels were quantified by real-time PCR and subsequently adjusted relative to control cells (n = 3 repeats/group). *G*, SENP3 overexpression inhibited EMT in both MDA-MB-231 and BT-549 cells. The sh-NC and sh-SENP3 plasmids were packaged and transduced into cells, followed by the detection of cellular lysates using immunoblotting with the specified antibodies. EMT, epithelial-mesenchymal transition; SENP, SUMO-specific protease; TNBC, triple-negative breast cancer.

group). The scale bar represents 20 μm. *H*, SENP3 knockdown significantly increased the invasive propensity of MDA-MB-231 cells. Evaluation of cell migration and invasion was conducted using a transwell assay with stably transfected cells (*left*). Migration and invasion cells were observed and analyzed (*right*, n = 5 replicates/group). The scale bar represents 20 μm. *I*, SENP3 knockdown promotes the unanchored growth of MDA-MB-231 cells. The formed sphere was calculated and analyzed (*right*, n = 5 repeats/group). The scale bar represents 20 μm. *J*, SENP3 knockdown promoted the transcription of stem cell markers in MDA-MB-231 cells. Gene transcript expression levels within cells were quantified by real-time PCR and subsequently adjusted relative to control cells (n = 3 repeats/group). *K*, SENP3 knockdown promoted EMT in both MDA-MB-231 and BT-549 cells. Both sh-NC and two sh-SENP3 plasmids were assembled and introduced into cells by transfection, and the cellular lysates were examined by immunoblotting using the specified antibodies. SENP, SUMO-specific protease; TNBC, triple-negative breast cancer.

epithelial cells (Fig. S3*A*). These results indicated high correlation of YAP1 and SENP3 protein in TNBC cells (Fig. S3*B*). Further experiments illustrated an increase in YAP1 expression after SENP3 elimination and a decrease in YAP1 expression after SENP3 overexpression (Fig. 3, *A* and *B*). Furthermore, the mRNA levels of downstream YAP1 genes increased with SENP3 knockdown and decreased with SENP3 overexpression in TNBC cells (Fig. 3, *C* and *D*). However, SENP3 did not show a significant effect on the level of YAP1 mRNA (Fig. 3, *C* and *D*). Coimmunoprecipitation (Co-IP) experiments revealed an interaction between exogenous YAP1 and SENP3 in HEK293T cells (Fig. 3, *E* and *F*) and endogenous YAP1 and SENP3 in MDA-MB-231 and BT549 cells (Fig. 3, *G* and *H*). In particular, the analysis of the database revealed that there is a negative correlation between the expression level of YAP1 and the survival of patients with TNBC (Fig. 3*I*). Furthermore, when examining samples from patients with TNBC, it was observed that the expression level of YAP1 was significantly higher in tissues with TNBC than in surrounding paracancerous tissues (Fig. 3*J*), suggesting a link between elevated YAP1 and TNBC progression.

To further identify the influence of YAP1 in SENP3-regulated TNBC, we knocked down SENP3 based on overexpression of YAP1 in MDA-MB-231 cells (Fig. S3, *C* and *D*). SENP3 knockdown increased cell proliferation in cancer cells overexpressing YAP1 (Fig. 3*K*). Additionally, SENP3 knockdown significantly improved colony formation and increased the migration and invasion of MDA-MB-231 cells overexpressing YAP1 (Fig. 3, *L*–*N*). The ability to form microspheres on soft agar was also improved with the elimination of SENP3 in cancer cells overexpressing YAP1 (Fig. 3*O*). Furthermore, YAP1 overexpression promoted the EMT process in cancer cells, and SENP3 suppression further accelerated the EMT process based on YAP1 overexpression (Fig. 3*P*). Taken together, these results suggested that SENP3 inhibition coupled with YAP1 overexpression promoted tumorigenesis in TNBC cells.

SENP3 knockdown promotes TNBC cell tumorigenesis in a YAP1-dependent manner

To verify the role of YAP1 in TNBC cells, we constructed MDA-MB-231 cells with stable knockdown of YAP1, followed by downregulation of downstream target genes of YAP1 (Fig. S4, *A*–*C*). MDA-MB-231 cell proliferation decreased after YAP1 knockdown (Fig. S4*D*). Furthermore, the colony formation assay demonstrated a weak clonogenic ability in MDA-MB-231 cells after YAP1 elimination (Fig. S4*E*). Migration and invasion were reduced after YAP1 knockdown in MDA-MB-231 cells (Fig. S4, *F* and *G*). We also found reduced sphere formation on soft agar after the elimination of YAP1, indicating the reduced ability of cells to grow unanchored (Fig. S4*H*). Detection of EMT markers revealed an increase in epithelial markers and a decrease in interstitial markers after the elimination of YAP1 in MDA-MB-231 cells (Fig. S4*I*). Therefore, YAP1 knockdown inhibited the invasion and EMT process of TNBC cells.

To elucidate the role of YAP1 in SENP3-regulated TNBC cells, we knocked down YAP1 in SENP3-deficient MDA-MB-231 cells (Fig. S4, *J* and *K*). The MTT assay showed that the elimination of YAP1 based on SENP3 knockdown decreased the proliferation of cancer cells (Fig. 4*A*). Additionally, clonal formation increased after YAP1 removal compared to control in SENP3-depleted TNBC cells (Fig. 4*B*). Scratch migration and transwell assays indicated decreased migration and invasion of MDA-MB-231 cells after YAP1 knockdown compared to the control in SENP3 knockdown cells (Fig. 4, *C* and *D*). We also found that after the knockdown of YAP1, there was a decrease in sphere formation on soft agar, indicating a reduction in unanchored growth capacity (Fig. 4*E*). Furthermore, the elimination of SENP3 promoted the EMT process, while the elimination of YAP1 rescued the EMT process with an increase in epithelial markers and a decrease in mesenchymal markers in MDA-MB-231 cells (Fig. 4*F*). Therefore, the elimination of YAP1 rescued the cell migration, invasion, and EMT process caused by SENP3 knockdown in TNBC, indicating that the elimination of SENP3 promotes the tumorigenesis of TNBC cells in a YAP1-dependent manner.

YAP1 is SUMOylated by SUMO1 and deSUMOylated by SENP3

YAP1 protein but not mRNA levels were regulated by SENP3 (Fig. 3, *A*–*D*), indicating that YAP1 is regulated by posttranslational modification. SENP3 acts as a specific enzyme for SUMOylation, suggesting its participation in the regulation of the SUMOylation homeostasis of YAP1. The SUMOplot database (www.abgent.com/sumoplot) suggested that YAP1 is highly likely to undergo SUMOylation (Fig. S5*A*). The Flag-YAP1 and HA-SUMO plasmids were cotransfected into HEK293T cells and co-IP experiments revealed that YAP1 is modified mainly by SUMO1 (Fig. 5*A*). Since the PIAS family comprises most of the SUMO E3 ligases, we cotransfected Flag-YAP1 and members of the PIAS family into HEK293T cells, and the results demonstrated that YAP1 had the strongest interaction with PIAS3 (Fig. 5*B*). Furthermore, the addition of PIAS3 enhanced YAP1 SUMOylation (Fig. 5*C*), while the knockdown of PIAS3 significantly decreased YAP1 SUMOylation (Fig. 5*D*). These results indicated that PIAS3 acts as the E3 ligase of YAP1, participating in the SUMOylation of YAP1. Next, we explored the effects of SENP3 on the YAP1 deSUMOylation process. Cotransfection of YAP1 with SUMO1 and WT or catalytic mutant SENP3 in HEK293T cells, and the results revealed that WT SENP3 deconjugated SUMOylation of YAP1, while this effect was retained in the presence of the catalytic mutant SENP3 (Fig. 5*E*). The SUMOylation site of YAP1 was predicted by the SUMOplot database, and the results showed that YAP1 had two potential SUMOylation sites, K97 and K280 (Fig. S5*A*). The mutant YAP1 plasmid at the SUMOylation site was generated and transfected into HEK293T cells, and the results showed that K280R significantly decreased the SUMOylation of YAP1 (Fig. 5*F*), and the K280 site is highly conserved in mammals (Fig. S5*B*). These results indicated that K280 is the main SUMOylation site of YAP1. Furthermore,

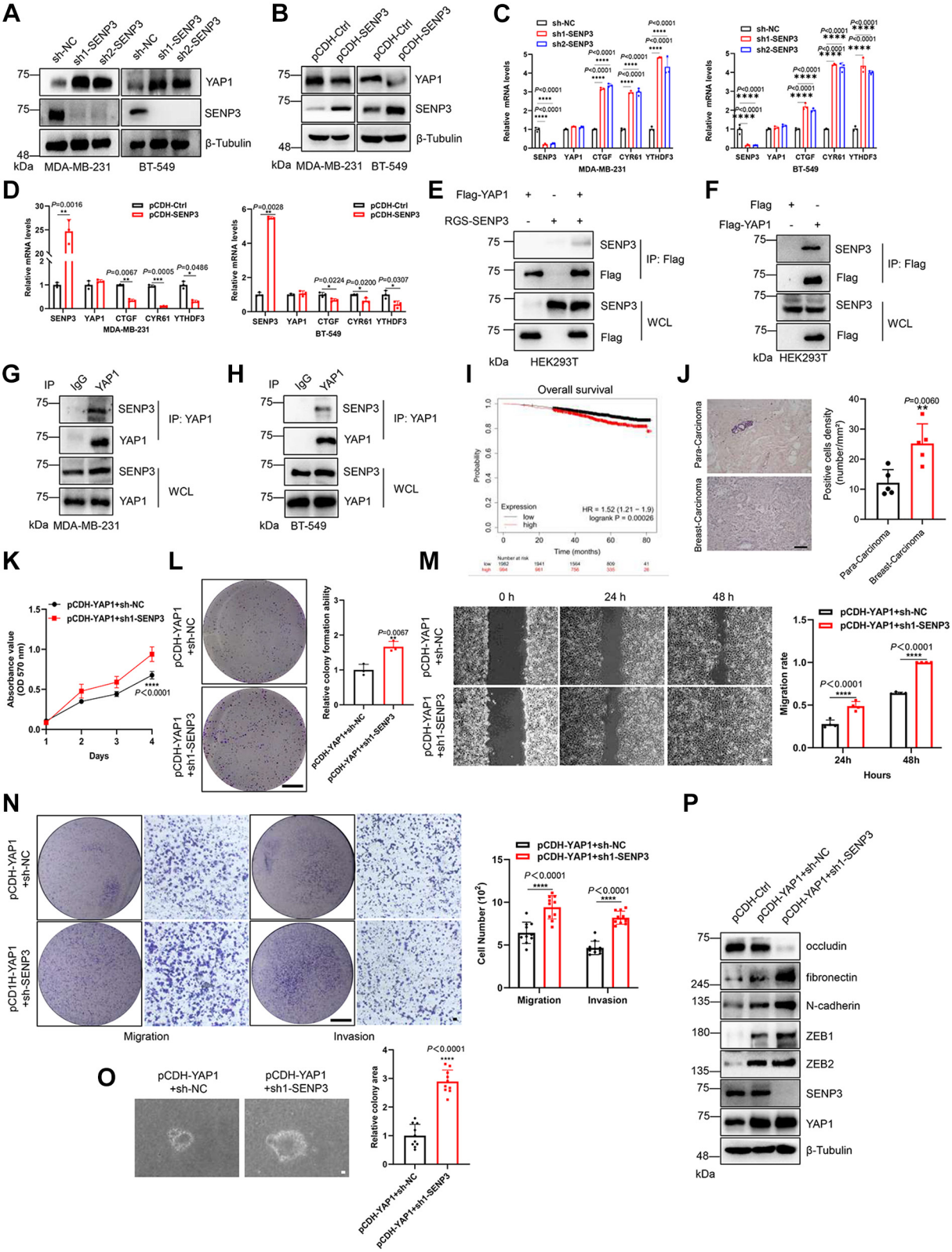

Figure 3. YAP1 acts as a downstream factor of SENP3 in the regulation of TNBC cells. *A*, SENP3 knockdown increased the protein expression level of YAP1. MDA-MB-231 and BT-549 cells were knocked down by two sh-SENP3, and WCL was analyzed by IB with the indicated antibodies. *B*, SENP3 overexpression decreased the expression level of the YAP1 protein. MDA-MB-231 and BT-549 cells were overexpressed by SENP3, and WCL was analyzed by IB with the indicated antibodies. *C*, SENP3 knockdown increased the transcription levels of the downstream genes of YAP1. MDA-MB-231 and BT-549 cells experienced a reduction in SENP3 expression, and gene transcript levels were quantified by real-time PCR and normalized to the control group (n = 3 repeats/group). *D*, SENP3 overexpression decreased the transcription levels of downstream YAP1 genes. MDA-MB-231 and BT-549 cells were induced to overexpress SENP3, and gene transcript levels were quantified by real-time PCR and normalized to the control group (n = 3 repeats/group). *E* and *F*, Both exogenous (*E*) and endogenous (*F*) SENP3 interacted with YAP1 in HEK293T cells. The Flag-YAP1 plasmid with (E) or without (*F*) RGS-SENP3 was introduced

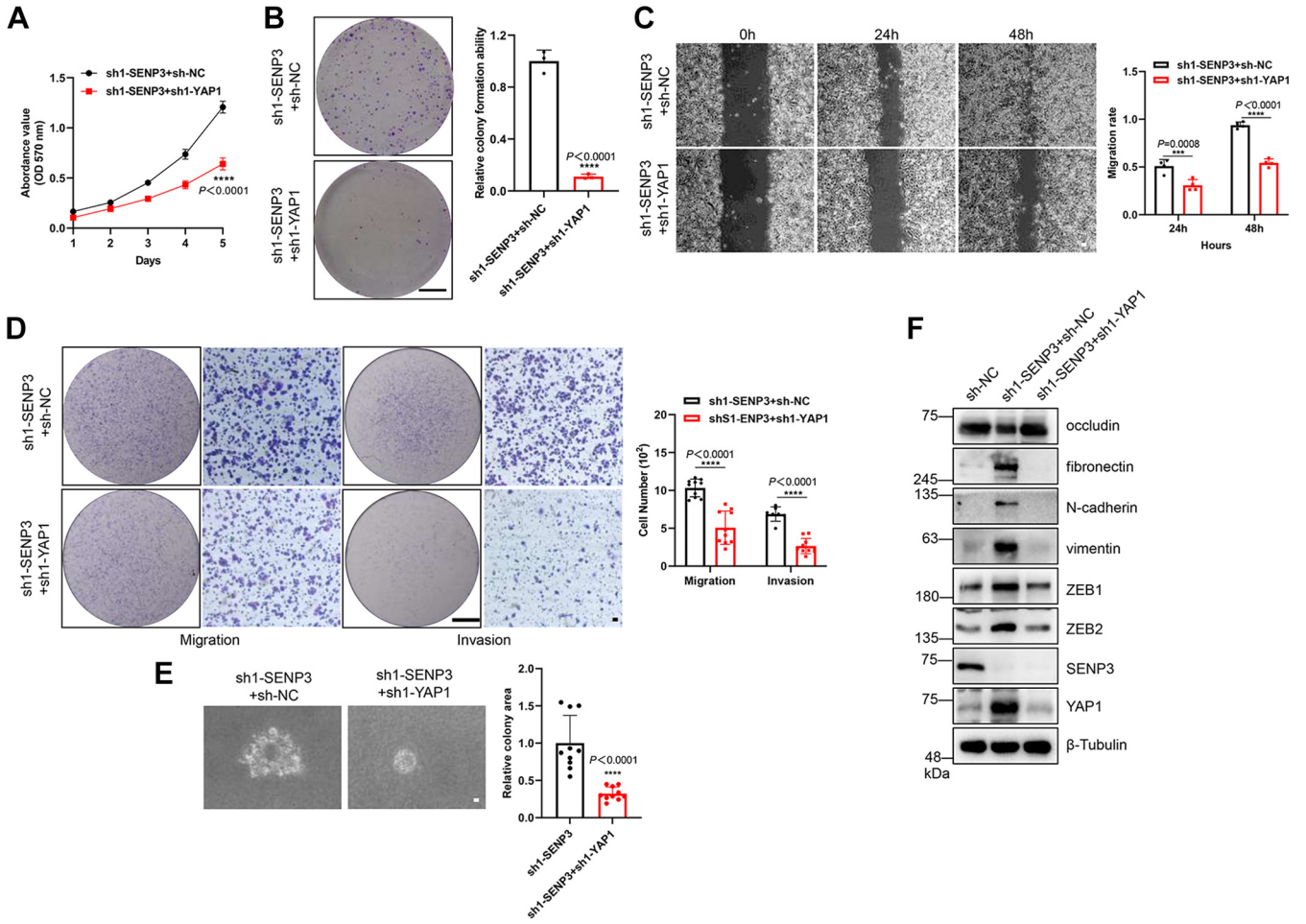

Figure 4. SENP3 knockdown regulates TNBC cells in a YAP1-dependent manner. *A*, YAP1 suppression decreased cell proliferation, which was increased by SENP3 knockdown. The growth curves of MDA-MB-231 cells subjected to YAP1 knockdown or maintained under control conditions were generated through daily quantification of cell number (n = 3 repeats/group). *B*, YAP1 knockdown decreased colony formation, which was increased by SENP3 suppression. MDA-MB-231 cells were seeded in a 24-well plate and cultured for 2 weeks, after which they were subjected to crystal violet staining for the colony formation assay (*left*). The colony formation capacity was analyzed (*right*, n = 3 repeats/group). The scale bar represents 200 μm. *C*, YAP1 knockdown inhibited cell migration that was promoted by SENP3 suppression. Migration of MDA-MB-231 cells was determined by a wound healing assay in stably transfected cells (*left*). The migration rate was measured and analyzed (*right*, n = 4 repeats/group). The scale bar represents 20 μm. *D*, YAP1 knockdown inhibited cell invasion that was promoted by SENP3 suppression. Migration and invasion of MDA-MB-231 cells were analyzed by transwell assay in stably transfected cells (*left*). The migration and invasion of cells were measured and analyzed (*right*, n = 10 repeats/group). The scale bar represents 200 μm (*left*) and 20 μm (*right*). *E*, YAP1 knockdown decreased the unanchored growth of MDA-MB-231 cells, which was increased by SENP3 suppression. The formed *sphere* was detected (*left*) and analyzed (*right*, n = 10 repeats/group). The scale bar represents 20 μm. *F*, YAP1 knockdown inhibited the EMT process of MDA-MB-231 cells that was promoted by SENP3 suppression. The sh-SENP3 and sh-YAP1 lentiviruses were packaged and infected into cells, and whole-cell lysates were detected by IB with the indicated antibodies. EMT, epithelial-mesenchymal transition; SENP, SUMO-specific protease; TNBC, triple-negative breast cancer.

into HEK293T cells and IP using anti-Flag antibody in whole-cell lysates was subjected to IB analysis with anti-SENP3 and anti-Flag antibodies. The WCL was detected by IB with anti-SENP3 and anti-Flag antibodies. *G* and *H*, endogenous SENP3 interacted with endogenous YAP1 in both MDA-MB-231 (*G*) and BT-549 (*H*) cells. The protein of MDA-MB-231 (*G*) and BT-549 (*H*) cells was harvested and IP with anti-YAP1 from cell lysates was detected by IB with anti-SENP3 and anti-YAP1 antibodies. The WCL was analyzed by IB with anti-SENP3 and anti-YAP1 antibodies. *I*, YAP1 expression was negatively correlated with the overall survival of patients with TNBC. YAP1 expression levels in TNBC tissue and normal tissue were analyzed with the GEPIA2 database. *J*, YAP1 was highly expressed in tissues from TNBC patients. YAP1 in cancer and precancerous tissue from TNBC patients was analyzed and calculated by immunohistochemistry with anti-YAP1 antibody (n = 5). Hematoxylin (*blue*) was applied to show the nuclei. The scale bar represents 50 μm. *K*, SENP3 knockdown facilitated YAP1 to promote the proliferation of MDA-MB-231 cells. Growth curves of cells subjected to SENP3 knockdown and control conditions were generated by daily quantification of cell number (n = 3 repeats/group). *L*, SENP3 knockdown facilitated YAP1 to increase the colony formation of MDA-MB-231 cells. The indicated cells were cultured and seeded in a 24-well plate for 2 weeks and stained with 0.1% crystal violet for the colony formation assay (*left*). The analysis of colony formation capacity was conducted (n = 3 repeats/group). The scale bar represents 200 μm. *M*, SENP3 knockdown facilitated YAP1 to enhance the migratory potential of MDA-MB-231 cells. Cell migration was assessed through a wound-healing assay carried out on stably transfected cells (*left*). The migration rate was calculated and analyzed (*right*, n = 4 repeats/group). The scale bar represents 20 μm. *N*, SENP3 knockdown facilitated YAP1 to increase the invasive capacity of MDA-MB-231 cells. Evaluation of cell migration and invasion was performed through a transwell assay in stably transfected cells (*left*). The migration and invasion of cells were measured and analyzed (*right*, n = 10 repeats/group). The scale bar represents 200 μm (*left*) and 20 μm (*right*). *O*, SENP3 knockdown facilitated YAP1 to enhance the unanchored growth of MDA-MB-231 cells. The formed *sphere* was observed (*left*) and analyzed (*right*, n = 10 repeats/group). The scale bar represents 20 μm. *P*, SENP3 knockdown facilitated YAP1 to enhance the EMT process of MDA-MB-231 cells. The pCDH-YAP1 and sh-SENP3 lentiviruses were packaged and transduced into cells, and whole-cell lysates were detected by IB with the indicated antibodies. IB, immunoblotting; EMT, epithelial-mesenchymal transition; SENP, SUMO-specific protease; TNBC, triple-negative breast cancer.

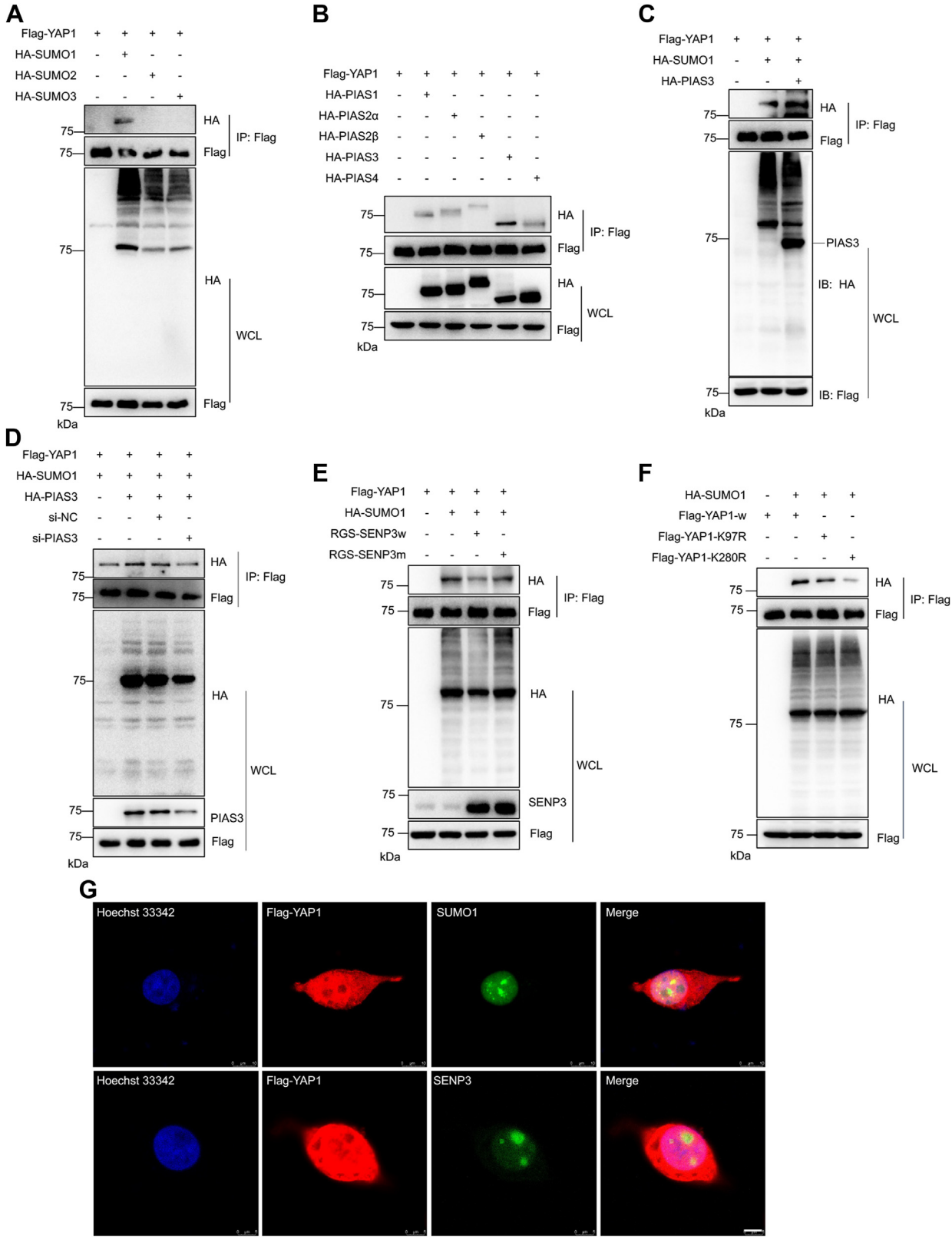

Figure 5. SUMO1 and SENP3 synergistically regulate the SUMOylation homeostasis of YAP1. *A*, YAP1 predominantly undergoes SUMOylation by SUMO1 in HEK293T cells. The indicated plasmids were transfected into HEK293T cells, and IP with anti-Flag from whole-cell lysates was subsequently identified by IB with anti-HA and anti-Flag antibodies. The WCL was analyzed by IB with anti-HA and anti-Flag antibodies. *B*, PIAS3 interacted with YAP1 in HEK293T cells. The designated plasmids were introduced into HEK293T cell substrates and IP using anti-Flag antibodies was performed on WCL, followed by IB using anti-HA and anti-Flag antibodies. The WCL was analyzed by IB with anti-HA and anti-Flag antibodies. *C*, PIAS3 markedly increased the SUMOylation of YAP1. The specified plasmids were introduced into HEK293T cellular substrates and IP was carried out using anti-Flag antibodies in cellular lysates, which were subsequently identified through IB using anti-HA and anti-Flag antibodies. Additionally, the analysis of WCL was carried out by IB employing anti-HA and anti-Flag antibodies. *D*, PIAS3 knockdown diminished the SUMOylation of YAP1. si-PIAS3 or the control was cotransfected with the specified plasmids in

immunofluorescence staining in HEK293T cells demonstrated colocalization of YAP1 with SUMO1 in the cell nucleus and YAP1 with SENP3 in the nucleolus (Fig. 5*G*). Taken together, these results showed that YAP1 is SUMOylated by SUMO1 with E3 PIAS3 and deconjugated by SENP3.

SUMOylation inhibits the ubiquitination of YAP1 and enhances its stability

SUMOylation has been shown to regulate the stability of target proteins and thus affect their functions (36, 37). The possible role of SUMOylation in the stability of YAP1 was explored. After cycloheximide (CHX) treatment in HEK293T cells, the YAP1 protein decreased in a time-dependent manner, with a half-life of approximately 6 h (Fig. S6*A*). The YAP1 and SUMO1 plasmids were cotransfected into HEK293T cells, followed by CHX treatment for 6 h prior to protein extraction, and the results showed that SUMOylation significantly inhibited YAP1 degradation (Fig. 6*A*), while the addition of SENP3 led to a significant degradation of the YAP1 protein (Fig. 6*B*). YAP1 with mutation of the SUMOylation site K280 showed faster degradation than WT YAP1, regardless of whether SUMO1 was present (Figs. 6*C* and S6*B*). Furthermore, after SENP3 overexpression, the degradation of WT YAP1 was equivalent to that of SUMO mutant YAP1 (Fig. S6*C*). These results indicated that SUMOylation of YAP1 enhanced its stability.

Previous studies have shown that YAP1 is degraded through the ubiquitin–proteasomal pathway (32). To further explore the effect of SUMOylation on YAP1 degradation, MG132, an inhibitor of the ubiquitin–proteasome pathway, was used to detect YAP1 stability. The stability of YAP1 increased after MG132 treatment, regardless of whether SUMO1 transfection was performed (Fig. 6*D*). SENP3 decreased the stability of YAP1, while MG132 treatment counteracted this effect (Fig. 6*E*). The degradation of the SUMO mutant YAP1 was also reversed by treatment with MG132 (Fig. 6*F*). The role of SUMOylation of YAP1 in its ubiquitination was detected, and the co-IP results showed that the ubiquitination of YAP1 was significantly reduced by SUMOylation (Fig. 6*G*). SENP3 cotransfection increased both the exogenous and endogenous ubiquitination of YAP1 (Fig. 6, *H* and *I*). Mutation at the SUMOylation site also improved the ubiquitination level of YAP1 (Fig. 6*J*). RNF4 is a major SUMO-targeted ubiquitin ligase and shows a strong interaction with YAP1 (Fig. S6*F*). Collectively, these results suggested that deSUMOylation of YAP1 promoted its ubiquitination and decreased protein stability. Furthermore, YAP1 in the nucleus increased after SENP3 suppression (Fig. 6*K* and S6*D*), whereas nuclear localization decreased after SENP3 overexpression (Fig. 6*L* and S6*E*). Taken together, these results suggested that SENP3 promoted SUMOylation-mediated ubiquitination-regulated degradation of YAP1.

SUMOylation of YAP1 drives the migration and invasion of TNBC cells

Since SENP3 regulates YAP1 SUMOylation and is negatively correlated with YAP1 expression, it prompts us to identify the effect of YAP1 SUMOylation on TNBC cells. We established MDA-MB-231 cell lines that stably overexpressed WT or SUMOylation site mutant YAP1, and the results showed that SUMO mutant YAP1 inhibited cell growth and colony formation that was accelerated by WT YAP1 (Fig. 7, *A* and *B*), suggesting that YAP1 SUMOylation promoted TNBC cell proliferation. Additionally, the SUMO mutant YAP1 decreased cell migration and invasion, which increased with WT YAP1 in MDA-MB-231 cells (Fig. 7, *C* and *D*), indicating that SUMOylated YAP1 contributes to cell migration and invasion. SUMO-deficient YAP1 inhibited the ability of cells to form spheres on soft agar that increased with WT YAP1 (Fig. 7*E*), indicating that YAP1 SUMOylation promoted the unanchored growth of TNBC cells. The effect of YAP1 SUMOylation on the EMT of TNBC cells was detected, and the results indicated that the SUMO mutant YAP1 significantly inhibited the EMT process promoted by WT YAP1 (Fig. 7*F*), indicating that YAP1 SUMOylation promoted the EMT process of TNBC cells. Furthermore, immunofluorescence staining and cell fraction analysis showed that WT YAP1 was mainly localized in the nucleus, whereas the SUMOylation site mutant YAP1 was localized in the cytoplasm of TNBC cells (Fig. 7, *G* and *H*). Additionally, the mutant YAP1 decreased the expression level of downstream genes that was increased by WT YAP1 (Fig. 7*I*). Subsequently, we extended our inquiry to *in vivo* models by examining the impact of SUMO mutation of YAP1 on the tumorigenesis of MDA-MB-231 cells in severe combined immunodeficiency (SCID) mice. Notably, WT YAP1 significantly enhanced the initiation and progression of subcutaneous xenografts in SCID mice, whereas SUMO mutation of YAP1 ameliorated the progression of xenografts, as evidenced by the growth curve and tumor weight (Fig. 7, *J–L*). These results indicate that SUMOylation of YAP1 plays a pivotal role in the promotion of carcinogenesis of TNBC. Taken together, these results indicate that SUMOylated YAP1 promotes cell migration, invasion, and EMT in TNBC cells.

Discussion

Effective management of TNBC presents a significant clinical challenge with unidentified key driver genes and signaling

HEK293T cells. IP using anti-Flag antibodies from whole cell lysates was determined by IB with anti-HA and anti-Flag antibodies. The WCL was analyzed by IB with the indicated antibodies. *E*, SENP3 facilitated the deconjugation of SUMOylation from YAP1 within HEK293T cells. The designated plasmids were introduced into HEK293T cells, and IP using anti-Flag antibody from whole-cell lysates was followed by IB with anti-HA and anti-Flag antibodies. The WCL was detected through IB using the specified antibodies. *F*, K280 was the primary SUMOylation site of YAP1. The WT and SUMO site mutant Flag-YAP1, along with HA-SUMO1, was introduced into HEK293T cells, and IP using anti-Flag antibody from whole-cell lysates was detected by IB employing anti-HA and anti-Flag antibodies. The WCL was detected by IB with anti-HA or anti-Flag antibodies. *G*, YAP1 exhibits nuclear colocalization with both SUMO1 and SENP3. The Flag-YAP1 plasmid was introduced into HEK293T cells, and these cells were subjected to immunofluorescence staining, using anti-YAP1 (*red*) and anti-SUMO1 or anti-SENP3 antibodies (*green*). The 4′,6-diamidino-2-phenylindole (*blue*) was used to show the nuclei. The scale bar represents 5 μm. EMT, epithelial-mesenchymal transition; IP, immunoprecipitation; SENP, SUMO-specific protease; TNBC, triple-negative breast cancer.

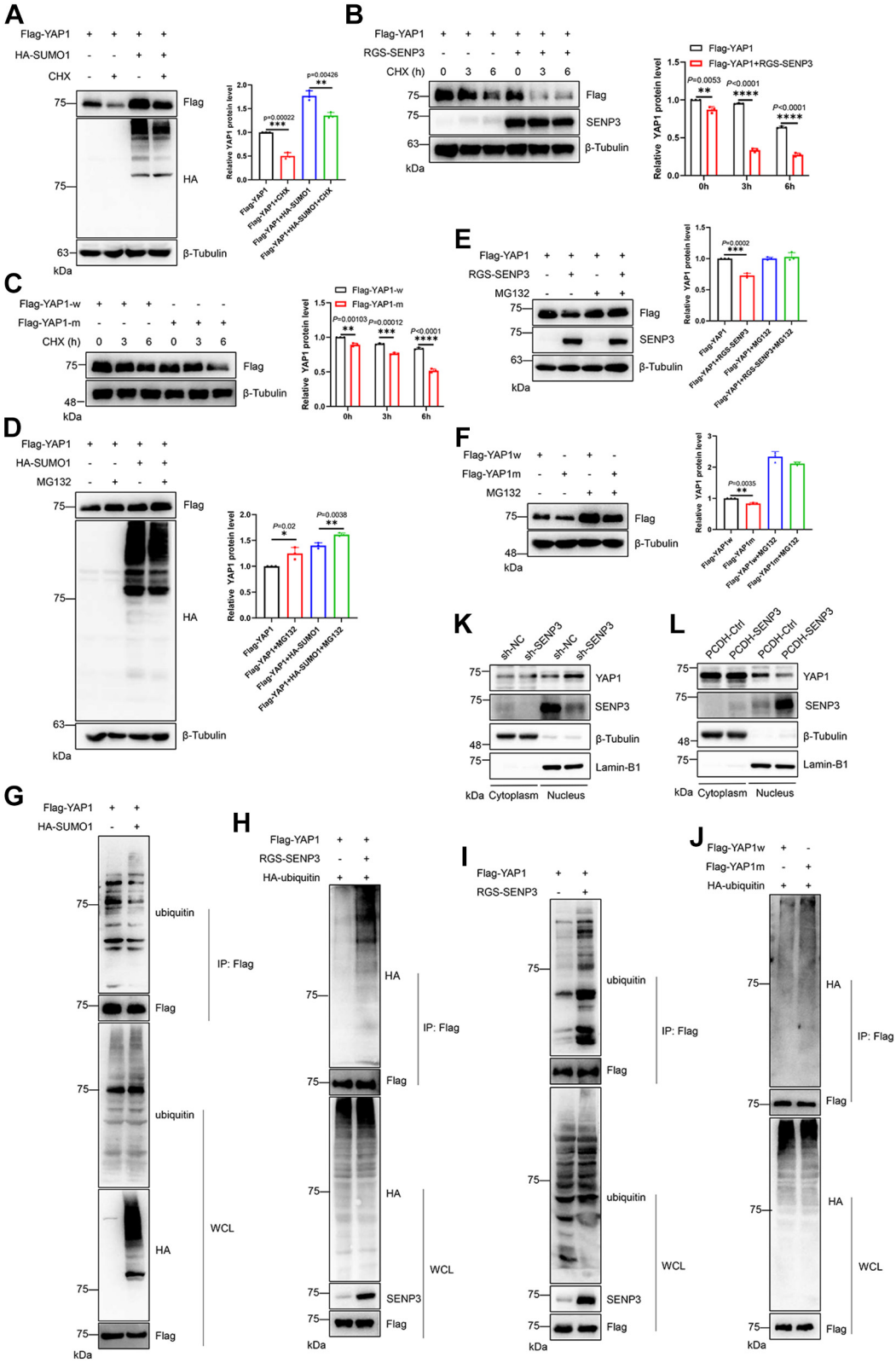

Figure 6. SUMOylation of YAP1 inhibits ubiquitin-proteasome–regulated degradation of YAP1. *A*, SUMOylation exerted a restraining influence on the degradation of the YAP1 protein. HEK293T cells were subjected to transfection with Flag-YAP1 and HA-SUMO1 plasmids and cells were treated with cycloheximide for 6 h. After treatment, the cells were harvested, and the resulting whole-cell lysates were subsequently subjected to immunoblotting with the designated antibodies (*left*). The results were measured and analyzed (*right*, n = 3 repeats/group). *B*, SENP3 facilitated the degradation of the YAP1 protein. HEK293T cells were transfected with Flag-YAP1 and RGS-SENP3 plasmids and cells were subjected to a 6-h treatment with CHX. After treatment, the cells were harvested, and the whole-cell lysates were subsequently subjected to IB using the specified antibodies (*left*). The results were measured and analyzed (*right*, n = 3 repeats/group). *C*, SUMO site mutant YAP1 promoted its degradation. Both WT and SUMO mutant YAP1 were introduced into HEK293T cells. Subsequently, the cells underwent CHX treatment for varying durations. After treatment, cells were harvested and the resulting cell lysates were

pathways. SENP3 has become an oxidative stress sensor and accumulates under worm oxidative stress (38). Previous investigations have reported that SENP3 is involved in various cancers, highlighting its significant role in tumorigenesis (39). Previous studies in a murine model indicated that the decrease in SENP3 contributed to macrophage polarization, thus advancing breast tumor progression (24). However, another study showed a contradictory role of SENP3 in breast cancer (25). Here, we address the critical role and molecular mechanism of SENP3 in TNBC, and the results indicated that SENP3 deconjugates the SUMOylation of YAP1 and promotes degradation mediated by the ubiquitin–proteasome system. However, the loss of SENP3 improved SUMOylation of YAP1, increasing stability and nuclear translocation and promoting progression of TNBC (Fig. 8).

To explore the intricate molecular mechanism through which SENP3 inhibits TNBC tumorigenesis, our focus expanded to the Hippo signaling pathway due to its relevance in various cancers, including breast cancer (40). The role of YAP1, a pivotal intermediate transkinase responder within the Hippo signaling pathway, plays a critical role in mammary gland–related functions. YAP1 acts as a promoter of adhesion plaque formation and tumor aggressiveness in breast cancer (41). Furthermore, suppression of HMGA2 inhibited the Hippo–YAP pathway, leading to attenuation of TNBC migration and *in vivo* tumor metastasis (42). Furthermore, YAP1 undergoes modification by SUMO1, although the precise mechanism of SUMO-mediated regulation remains unknown (43). Given this, we directed our attention to scrutinizing the impact of SENP3-regulated YAP1 SUMOylation on TNBC. In our study, we not only validated a highly specific interaction between YAP1 and SUMO1 in TNBC but also revealed the homeostasis of YAP1 SUMOylation equilibrium by SENP3 and PIAS3 (Figs. 3–5). Our findings showed that SENP3 deficiency promoted TNBC progression in a YAP1-dependent manner, elucidating the pivotal role of SUMOylation-regulated activation of the Hippo–YAP1 pathway in TNBC tumorigenesis.

Regulation of YAP1 stability is essential for the Hippo–YAP pathway. Phosphorylation of YAP1 by the upstream kinases LAST1/2 prompts its cytoplasmic accumulation and degradation *via* the ubiquitin–proteasomal pathway. On the contrary, unphosphorylated YAP1 translocates to the nucleus, orchestrating the activation of its downstream target genes as transcriptional cofactors (44). SUMOylation plays a critical role in the regulation of target protein stability (36). We explored the influence of SUMOylation on YAP1 stability, revealing that SUMOylation improves YAP1 stability and *vice versa* by deSUMOylation (Fig. 6). Specifically, our results indicated that SUMOylation leads to ubiquitination of YAP1, followed by ubiquitin-proteasomal degradation, whereas SENP3 deconjugated SUMOylation of YAP1 and resulted in inhibition of ubiquitination and degradation of YAP1 (Fig. 6). Our findings validated the regulatory interaction of YAP1 between ubiquitination and SUMOylation. Enhanced SUMOylation promotes YAP1 stability and subsequently promotes nuclear translocation by dampening YAP1 ubiquitination.

In summary, our results unveiled the critical role of SENP3 as a tumor suppressor gene in TNBC cells. SENP3 overexpression inhibits TNBC cell migration and EMT in a YAP1-dependent manner. In particular, YAP1 was SUMOylated by SUMO1, whereas SENP3 overexpression curbs YAP1 expression in the nucleus, concurrently suppresses downstream factors of the Hippo–YAP1 pathway, and effectively retards the onset and progression of TNBC. Collectively, our findings elucidate the intricate molecular mechanism by which SENP3 impacts the TNBC trajectory by orchestrating YAP1 degradation through deSUMOylation. These insights not only provide a fresh theoretical foundation but also present a molecular target for therapeutic intervention in patients with TNBC.

Experimental procedures

Cell culture and treatment

The human embryonic kidney cell lines HEK293T and HEK293TN, the human mammary epithelial cell line MCF-10A, and the TNBC cell lines BT-549 and MDA-MB-231 were purchased from American Type Cell Collection. These cells were cultured in Dulbecco's modified Eagle's medium (Thermo Fisher Scientific) supplemented with 10% fetal bovine serum (Thermo Fisher Scientific) and 1% penicillin and streptomycin (Invitrogen), and were meticulously maintained

analyzed by immunoblotting with anti-Flag and anti-β-tubulin antibodies (*left*). The results were calculated (right, n = 3 repeats/group). *D*, MG132 facilitates SUMO1 inhibition of YAP1 protein degradation. HEK293T cells were transfected with Flag-YAP1 and HA-SUMO1 plasmids, and then the cells were subjected to a 4-h treatment with MG132. After treatment, the cells were harvested, and the whole-cell lysates were subsequently subjected to IB using the designated antibodies (*left*). The results were calculated (*right*, n = 3 repeats/group). *E*, MG132 inhibits the degradation of the YAP1 protein induced by SENP3. HEK293T cells were transfected with Flag-YAP1 and RGS-SENP3 plasmids and then the cells were subjected to 4-h treatment with MG132. After treatment, the cells were harvested, and the resultant cell lysates were subsequently subjected to IB using the designated antibodies (*left*). The results were measured and analyzed (*right*, n = 3 repeats/group). *F*, MG132 inhibits the degradation of the mutant SUMOylation site YAP1. WT or SUMO mutant YAP1 was transfected into HEK293T cells, and the cells were treated with MG132 for 4 h. Cells were harvested and whole-cell lysates were detected by IB with anti-Flag and anti-β-tubulin antibodies (*left*). The results were calculated (*right*, n = 3 repeats/group). *G*, SUMOylation of YAP1 inhibited its ubiquitination. Plasmids carrying Flag-YAP1 and HA-SUMO1 were introduced into HEK293T cells and IP using anti-Flag antibodies from whole-cell lysates was determined using IB employing anti-ubiquitin and anti-Flag antibodies. The WCL were subjected to IB using the specified antibodies. *H–I*, SENP3 promoted the exogenous (*H*) and endogenous (*I*) ubiquitination of YAP1. The indicated plasmids were introduced into HEK293T cells, and then IP with anti-Flag of whole-cell lysates was detected by IB with the indicated antibodies, and WCL was detected by IB with the indicated antibodies. *J*, SUMO site mutant YAP1 promoted its ubiquitination. WT and SUMO site mutant YAP1 were transfected with HA-ubiquitin into HEK293T cells, and IP using anti-Flag antibodies from whole-cell lysates was followed by IB using anti-HA and anti-Flag antibodies. The WCL were subjected to IB employing anti-HA and anti-Flag antibodies. *K*, SENP3 knockdown promoted the nuclear localization of YAP1. The fraction of MDA-MB-231 cells with SENP3 knockdown was detected by IB with indicated antibodies. *L*, SENP3 overexpression inhibited the nuclear localization of YAP1. The fraction of MDA-MB-231 cells overexpressing SENP3 was detected by IB with indicated antibodies. SENP, SUMO-specific protease; TNBC, triple-negative breast cancer; EMT, epithelial-mesenchymal transition; CHX, cycloheximide; IP, immunoprecipitation.

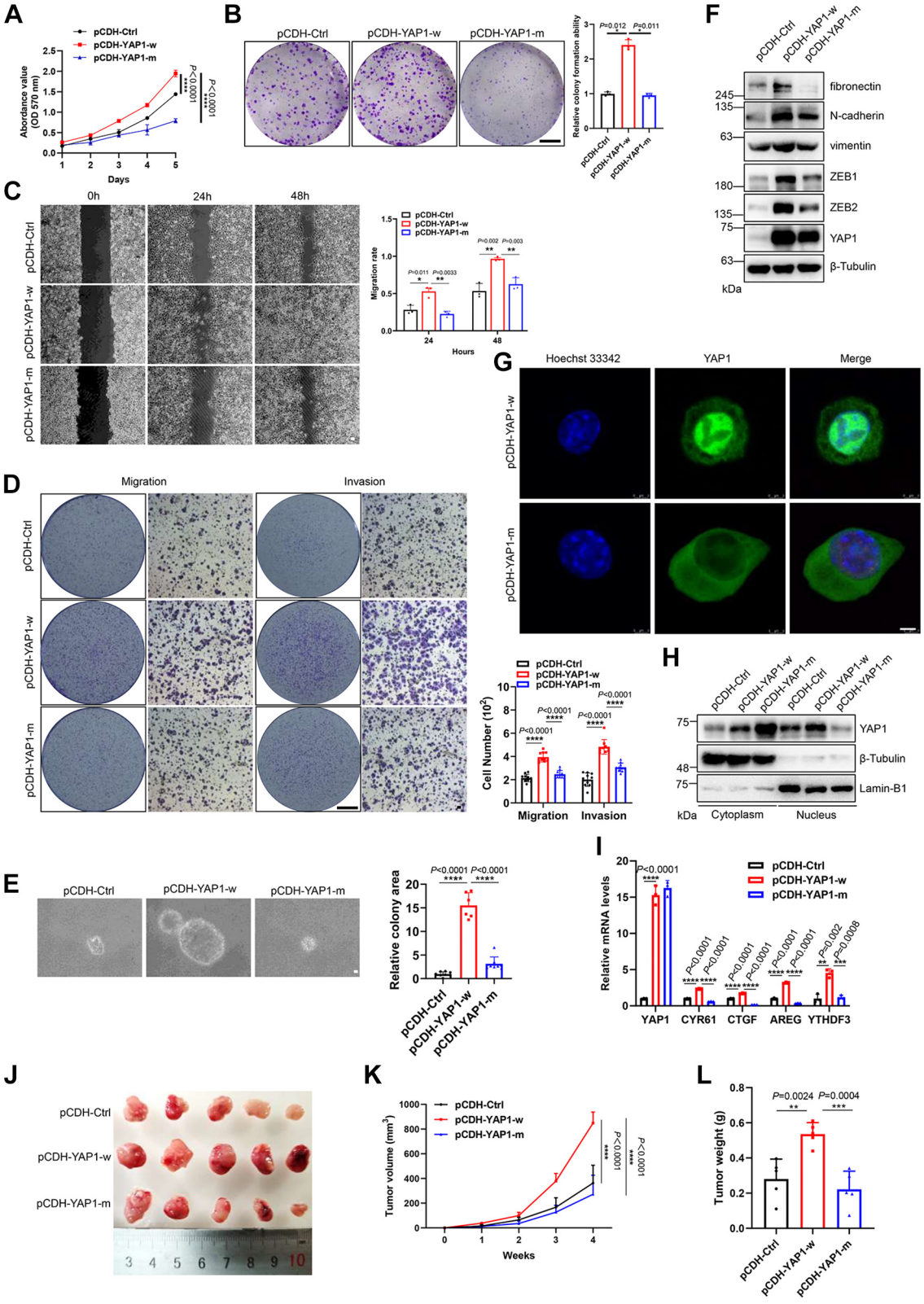

Figure 7. Mutation of the SUMOylation site of YAP1 affects the function of WT YAP1 in MDA-MB-231 cells. *A*, SUMO site mutant YAP1 decreased cell proliferation, which was increased by WT YAP1. Growth curves were generated and quantified for cells with YAP1 overexpression and control MDA-MB-231 cells (n = 3 repeats/group). *B*, SUMO site mutant YAP1 decreased colony formation, which was increased by WT YAP1. MDA-MB-231 cells were seeded in a 24-well plate for 2 weeks and stained with 0.1% crystal violet for the colony formation assay (*left*). The colony formation capacity was analyzed (*right*, n = 3 repeats/group). The scale bar represents 200 μm. *C*, SUMO site mutant YAP1 inhibited cell migration promoted by WT YAP1. Migration of MDA-MB-231 cells was determined by a wound healing assay in stably transfected cells (*left*). The migration rate was measured and analyzed (*right*, n = 3 repeats/group). The scale bar represents 20 μm. *D*, SUMO site mutant YAP1 inhibited cell invasion that was promoted by WT YAP1. Migration and invasion of MDA-MB-231 cells were analyzed by transwell assay in stably transfected cells (*left*). The migration and invasion cells were observed and analyzed (*right*, n = 10 repeats/group).

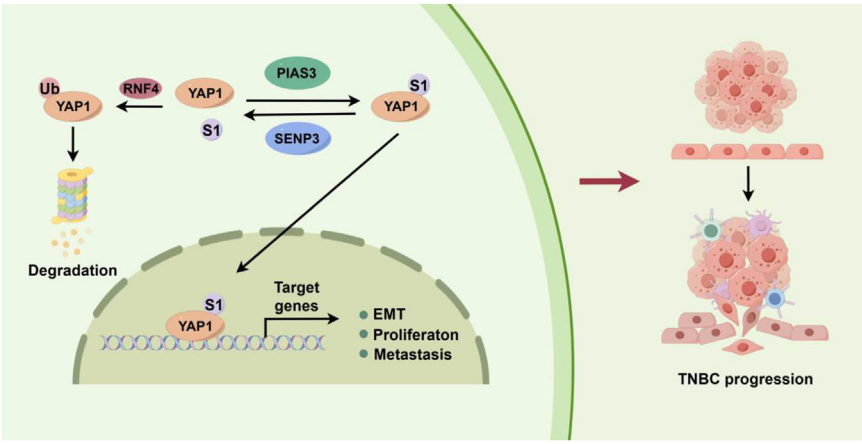

Figure 8. SENP3 mediates the deSUMOylation of YAP1 to regulate the progression of TNBC. YAP1 is SUMOylated by SUMO1, and SENP3 deconjugates the SUMOylation of YAP1 and promotes ubiquitin-proteasomal degradation. SUMOylation of YAP1 facilitated its nuclear localization and transcription of downstream genes and promoted the proliferation, migration, and EMT of TNBC cells. SENP, SUMO-specific protease; TNBC, triple-negative breast cancer; EMT, epithelial-mesenchymal transition.

at 37 °C within a controlled atmosphere of 5% CO_2. For the CHX assay, cells were subjected to treatment with 50 μg/ml CHX for varying durations and whole-cell lysates (WCLs) were meticulously harvested and subjected to Western blotting.

Plasmid construction

HA-SUMO1, HA-SUMO2, RGS-SENP3, and the catalytic mutant RGS-SENP3 plasmids were generated in our laboratory. The Flag-YAP1 plasmid was kindly provided by Dr Dawang Zhou of Xiamen University, and the SUMO site mutation of YAP1 was generated using the Quick-change site–directed mutagenesis kit (Vazyme) with the indicated primers (Table S2). The pCDH-Puro plasmids were purchased from System Biosciences (SBI). The plasmid pLVX-sh-SENP3 was kindly provided by Dr Jing Yi from Shanghai Jiao Tong University. The plasmids pCDH-SENP3, pCDH-YAP1, and sh-YAP1 were constructed using the molecular cloning technique in the laboratory (Table S1). All plasmids were confirmed by DNA sequencing (Table S3).

Establishment of stable cell lines

Engineered cell models with gene knockdown or overexpression were constructed according to the protocol. Briefly, gene knockdown or overexpression lentivirus was obtained through the lentiviral packaging technique and incubated with TNBC cells in a 6-cm cell culture plate for 1 to 2 days, and the infected cells were cultured under puromycin treatment. The WCL was meticulously collected and analyzed by Western blotting to detect the efficiency of gene knockdown or overexpression.

Xenograft mouse models

Five-week-old female Bagg's albino/c SCID mice were purchased from Beijing Vital River Laboratory Animal Technology for experiments. The mice were housed at 22 °C with a 12-h light-dark cycle and given *ad libitum* access to food and water. A total of 4×10^6 control, pCDH-YAP1w or pCDH-YAP1m lentivirus transduced MDA-MB-231 cells were subcutaneously implanted into the left flank of the mice. Tumor growth was monitored by measuring the xenograft dimensions every 4 days, and the mice were observed daily. Tumor volumes were calculated using the formula: volume (mm^3) = 0.5 × longest tumor diameter × (shortest tumor diameter)^2. At the study endpoint, the mice were euthanized, and tumors were collected for weight. All procedures followed the "Guide for the Care and Use of Laboratory Animals" and were approved by the Institutional Animal Care and Use Committee of Shaanxi Normal University.

Cell viability assay

Cellular seeding was carried out at a density of 1000 cells per well within a 96-well plate, followed by incubation in cell culture medium. Subsequently, at time points of 24, 48, and 72 h, cell viability assessments were performed using MTT

The scale bar represents 200 μm (*left*) and 20 μm (*right*). *E*, SUMO site mutant YAP1 decreased the unanchored growth of MDA-MB-231 cells that was increased by WT YAP1. The formed *sphere* was detected (*left*) and analyzed (*right*, n = 6 repeats/group). The scale bar represents 20 μm. *F*, SUMO site mutant YAP1 inhibited the EMT process of MDA-MB-231 cells that was promoted by WT YAP1. The specified lentiviral vectors were packaged and introduced into the target cells. Subsequently, whole-cell lysates were analyzed by immunoblotting employing designated antibodies. *G*, SUMOylation of YAP1 promoted its localization in the nucleus. The indicated lentivirus was packaged and transduced into MDA-MB-231 cells and the cells were harvested for immunofluorescence with anti-YAP1 (*red*) antibody. The 4′,6-diamidino-2-phenylindole (*blue*) was used to show the nuclei. The scale bar represents 5 μm. *H*, SUMOylation of YAP1 promoted its translocation from the cytoplasm to the nucleus. The indicated lentivirus was packaged and transfected into MDA-MB-231 cells and the cell cytoplasm, and the nucleus lysates were detected by IB with the indicated antibodies. *I*, SUMO site mutant YAP1 showed a significant effect on the transcription levels of downstream genes. The indicated lentivirus was packaged and transfected into cells and the expression levels of gene transcripts were measured by real-time PCR and normalized to control cells (n = 3 repeats/group). *J–L*, SUMO site mutant YAP1 decreased tumorigenesis, which was increased by WT YAP1 of breast cancer *in vivo*. The tumor volume (*J–K*) and tumor weight (*L*) were measured every 4 days, and the tumors were harvested and weighed at the end of the experiment (n = 5 mice/group). SENP, SUMO-specific protease; TNBC, triple-negative breast cancer; EMT, epithelial-mesenchymal transition.

(Sigma) according to the manufacturer's instructions. In a succinct description, 20 μl of a 5 mg/ml MTT solution was introduced into each well, followed by a 4-h incubation period at 37 °C. After incubation, 150 μl of dimethyl sulfoxide (Thermo Fisher Scientific) was administered to each well and absorbance measurements were carried out using a multimode microplate reader (Thermo Fisher Scientific) set at 570 nm.

Colony formation assay

Cellular seeding was performed within 24-well plates, with each well receiving 200 cells. After overnight incubation, cells were treated with the designated agents and cultured at 37 °C in a humidified atmosphere of 5% CO_2 for 2 weeks. The culture medium was replenished every 3 days during the incubation period. Following incubation, the colonies that had developed were subjected to two rounds of PBS washes, followed by fixation with methanol for 15 min. Subsequently, staining was carried out utilizing a 0.1% crystal violet solution, and examination was performed under a microscope (Leica).

Wound healing assay

Cellular seeding was performed in 6-well plates, with each well receiving 5×10^5 cells. Once an 80% confluence threshold was reached, a mechanical wound was meticulously induced within the cell monolayer through gentle scratching using a sterile 200 μl pipette tip. After this, the cells were cultured in serum-free medium for varying durations. Subsequently, images of the wounded region were diligently captured using an inverted microscope (Leica), with subsequent quantification of the scratch width achieved utilizing ImageJ software (https://imagej.net). The average width of the scratch was calculated as the area of the scratch divided by the length. Relative width was determined as the width of the scratch divided by the initial width of the scratch width at 0 h.

Transwell migration and invasion assay

Transwell migration and invasion assays were performed with 24-well Boyden chamber transwell inserts (BD Biosciences) with Corning Matrigel added to the upper chamber at a concentration of 200 μg/ml. A total of 1.5×10^4 cells were added to the upper chamber in 150 μl of serum-free culture medium, while the lower chamber of each well contained 500 μl of culture medium supplemented with 10% fetal bovine serum. After 24 h of incubation at 37 °C in an incubator with 5% CO_2, cells that had migrated to the bottom of the upper chamber membrane were stained with 0.1% crystal violet and examined with the microscope (Leica).

Soft agar sphere-forming assay

Prepare an agarose gel by combining 750 μl of 1.2% agarose with 750 μl of preheated 2 × culture medium, thoroughly mix the solution, and spread it on a 6-well plate, allowing it to coagulate at room temperature for 1 h. Next, 2000 cells diluted in 750 μl of preheated 2 × culture medium and 0.7% agarose were added to the cell mixture. The contents were thoroughly mixed and the cell agarose mixture was carefully spread onto the upper layer of the 1.2% agarose gel. The plate was allowed to solidify at room temperature for 1 h. Following gel solidification, add 1 ml of complete culture medium on top of agarose and transfer the plate to an incubator. After a 2-week culture period, the tumor cell spheres were visualized under a microscope (Leica).

Immunocytochemistry

Cells that had been transfected with the designated plasmids were cultured on a coverslip for 48 h, after which they were meticulously subjected to PBS washing, fixation with 4% paraformaldehyde (PFA, Thermo Fisher Scientific), and permeabilization through Triton X-100. To minimize nonspecific antibody interactions, 10% goat serum (Thermo Fisher Scientific) was applied at room temperature. The primary antibodies were then incubated with the cells for 1 h at 37 °C. Subsequently, the cells were washed twice in PBS and then subjected to 1-h incubation at room temperature with secondary antibodies labeled with Alexa Fluor 488 or 546 fluorophores (Thermo Fisher Scientific). Following another three rounds of PBS washing, cells were incubated with 4′,6-diamidino-2-phenylindole for 10 min, followed by mounting using an antifade mounting solution (Dako, Glostrup). Subsequently, the examination was performed by confocal laser scanning microscopy (Leica).

mRNA isolation and real-time quantitative polymerase chain reaction

To allow a meticulous quantitative analysis of gene expression, the total mRNA pool was meticulously extracted from cultured or transfected cells using the RNeasy protocol (Solarbio). Following mRNA isolation, DNase (Promega) treatment was performed, with subsequent concentration determination achieved by detecting absorbance at 260 nm. Uniform mRNA levels were harnessed to facilitate the generation of complementary DNA, which was accomplished by the high-capacity complementary DNA reverse transcription assay (Thermo Fisher Scientific). Subsequently, quantitative real-time PCR was performed, featuring reaction mixtures comprising complementary DNA, primers (Table S4), and SYBR Green reagent (Thermo Fisher Scientific), employing the ABI StepOne system (PerkinElmer). The PCR process was conducted meticulously in triplicate, with SDs being computed to account for experimental variances. All acquired data were subjected to analysis using ABI PRISM software (www.thermofisher.cn/cn/en/home/technical-resources/software-downloads.html). This software serves to establish the threshold cycle and melt curve, which delineates the point at which the fluorescence intensity significantly surpasses the background fluorescence levels.

Extraction of nuclear and cytoplasmic protein

The transfected cells were harvested and washed with PBS, and premix lysis buffer was added to the cells and incubated on ice for 20 min. Subsequently, the mixture was centrifuged at 4 °C, and the supernatant was collected as the cytoplasmic protein fraction, The cellular fraction extraction kit (KeyGen) was used to isolate the nucleoprotein fraction. Briefly, the cell

pellet was treated with 100 μl of the precooled buffer. The mixture was shaken vigorously for 15 s, followed by incubation on ice for 60 min with intermittent shaking every 10 min. Subsequently, the sample was centrifuged at 4 °C and the supernatant was quickly transferred to a precooled EP tube to obtain the nucleoprotein.

Western blot and immunoprecipitation

Cell lysis was conducted on ice using radioimmunoprecipitation assay lysis buffer supplemented with protein inhibitors. After lysis, the quantification of total protein content was meticulously carried out using bicinchoninic acid analysis (Solarbio). Equal amounts of protein were subjected to electrophoresis and subsequently transferred onto the polyvinylidene fluoride membrane. Following membrane transfer, a blocking step ensued, followed by an overnight incubation with the primary antibody. After thorough washing steps, the membrane was exposed to the secondary antibody coupled with peroxidase, and the protein content was detected *via* a chemiluminescence system (Qinxiang). In the case of immunoprecipitation experiments, WCLs were subjected to overnight incubation with primary antibodies. The antibody-bound protein complex was then captured and subjected to incubation following the addition of protein G agarose. The precipitation of protein G agarose was achieved through centrifugation, and the immunoprecipitated protein complex was eluted with SDS-PAGE sample buffer. Subsequently, Western blotting was performed using the indicated antibodies (Table S5). All reagents and compounds are listed in Table S6.

Breast cancer specimens and immunohistochemistry staining

Breast cancer patients were diagnosed at the Affiliated Hospital of Southwest Medical University, and TNBC and adjacent noncancerous tissues were collected during surgeries for diagnostic and therapeutic purposes (Table S7). These preexisting specimens were not specifically obtained for the current study. With appropriate IRB (L2021012) approved by the Ethics Committee of the Affiliated Hospital of Southwest Medical University, paraffin-embedded sections of randomly selected breast cancer specimens were evaluated by immunohistochemistry (IHC) staining for YAP1 expression using an IHC kit (Vector Laboratories) according to the manufacturer's protocol. The studies in this work abide by the Declaration of Helsinki principles. For the quantitative analysis of IHC staining, ImageJ software (National Institutes of Health) was used to count the number of positive cells in tissue sections and imported for analysis.

Quantification and statistical analysis

Data are reported as the mean ± SD based on a minimum of three independent experiments. Group distinctions were assessed through two-group comparison tests, complemented by one-way ANOVA paired with either Dunnett's or Tukey's post hoc assessments. For scenarios involving more than two groups, two-way ANOVA was employed, followed by Bonferroni's post hoc analysis. Comparable variances were observed among the groups subjected to statistical comparison. Statistical significance was established at $p < 0.05$, denoted as $^{*}p < 0.05$, $^{**}p < 0.01$, $^{***}p < 0.001$, and $^{****}p < 0.0001$ for the respective levels of significance.

Data availability

The authors confirm that the data supporting the findings of this study are available within the article and its supplementary materials.

Supporting information—This article contains supporting information.

Acknowledgments—The authors are grateful to Dr Jing Yi from the Shanghai Jiao Tong University School of Medicine for kindly providing the pLvx-sh-SENP3 plasmid and Dr Dawang Zhou from Xiamen University for kindly providing the Flag-YAP1 plasmid.

Author contributions—X. C., D. L., and Q. S. writing–original draft; X. C., D. L., Q. S., Xing Ling, Y. Y., Y. L., X. Z., A. H., S. D., R. X., Z. L., and Xiaojun Long investigation; Xing Ling, Y. Y., Y. L., X. Z., A. H., S. D., R. X., Z. L., and Xiaojun Long validation; X. C., Q. S., S. D., Y. Q., and H. W. funding acquisition; X. C., D. L., and Q. S. formal analysis; X. C., D. L., and Q. S. data curation; J. Z. and Z. Y. resources; Y. Q. and H. W. writing–review and editing; Y. Q. and H. W. supervision; Y. Q. and H. W. conceptualization.

Funding and additional information—The research presented here received grants from the National Natural Science Foundation of China (Y. Q.: 81870241; H. W.: 82273395; and X. C.: 82203387), the Fundamental Research Funds for the Central Universities (Y. Q.: GK202202006; H. W.: GK202205009; and X. C.: GK202207003), the Shaanxi Provincial Postdoctoral Science Foundation (X. C.: 2023BSHYDZZ117), the Excellent Graduate Training Program of Shaanxi Normal University (Q. S.: LHRCTS23089 and S. D.: LHRCCX23174), and the Macao Youth Scholars Program (X. C.: AM2022017).

Conflict of interest—The authors declare that they have no conflict of interests with the contents of this article.

Abbreviations—The abbreviations used are: CHX, cycloheximide; Co-IP, coimmunoprecipitation; EMT, epithelial-mesenchymal transition; IHC, immunohistochemistry; MTT, 3-(4, 5-dimethylthiazol-2-yl)-2, 5-diphenyltetrazolium bromide; RNF, ring finger protein; SCID, severe combined immunodeficiency; SENP3, SUMO-specific protease 3; TNBC, triple-negative breast cancer; WCL, whole-cell lysate.

References

1. Brufsky, A., Valero, V., Tiangco, B., Dakhil, S., Brize, A., Rugo, H. S., *et al.* (2012) Second-line bevacizumab-containing therapy in patients with triple-negative breast cancer: subgroup analysis of the RIBBON-2 trial. *Breast Cancer Res. Treat* **133**, 1067–1075
2. Ribatti, D., Nico, B., Ruggieri, S., Tamma, R., Simone, G., and Mangia, A. (2016) Angiogenesis and antiangiogenesis in triple-negative breast cancer. *Transl. Oncol.* **9**, 453–457
3. Speiser, J., Foreman, K., Drinka, E., Godellas, C., Perez, C., Salhadar, A., *et al.* (2012) Notch-1 and Notch-4 biomarker expression in triple-negative breast cancer. *Int. J. Surg. Pathol.* **20**, 139–145

4. Salimi, M., and Sedaghati Burkhani, S. (2019) Integrity and quantity evaluation of plasma cell-free DNA in triple negative breast cancer. *Avicenna. J. Med. Biotechnol.* **11**, 334–338
5. Yue, C. H., Liu, J. Y., Chi, C. S., Hu, C. W., Tan, K. T., Huang, F. M., *et al.* (2019) Myeloid zinc finger 1 (MZF1) maintains the mesenchymal phenotype by down-regulating IGF1R/p38 MAPK/ERalpha signaling pathway in high-level MZF1-expressing TNBC cells. *Anticancer Res.* **39**, 4149–4164
6. Zhang, L., Du, Y., Xu, S., Jiang, Y., Yuan, C., Zhou, L., *et al.* (2019) DEPDC1, negatively regulated by miR-26b, facilitates cell proliferation via the up-regulation of FOXM1 expression in TNBC. *Cancer Lett.* **442**, 242–251
7. Dent, R., Trudeau, M., Pritchard, K. I., Hanna, W. M., Kahn, H. K., Sawka, C. A., *et al.* (2007) Triple-negative breast cancer: clinical features and patterns of recurrence. *Clin. Cancer Res.* **13**, 4429–4434
8. Cancer Genome Atlas, N. (2012) Comprehensive molecular portraits of human breast tumours. *Nature* **490**, 61–70
9. van 't Veer, L. J., Dai, H., van de Vijver, M. J., He, Y. D., Hart, A. A., Mao, M., *et al.* (2002) Gene expression profiling predicts clinical outcome of breast cancer. *Nature* **415**, 530–536
10. He, J., Peng, T., Peng, Y., Ai, L., Deng, Z., Wang, X. Q., *et al.* (2020) Molecularly engineering triptolide with aptamers for high specificity and cytotoxicity for triple-negative breast cancer. *J. Am. Chem. Soc.* **142**, 2699–2703
11. Zhou, H., Mohamedali, K. A., Gonzalez-Angulo, A. M., Cao, Y., Migliorini, M., Cheung, L. H., *et al.* (2014) Development of human serine protease-based therapeutics targeting Fn14 and identification of Fn14 as a new target overexpressed in TNBC. *Mol. Cancer Ther.* **13**, 2688–2705
12. Tariq, K., Farhangi, A., and Rana, F. (2014) TNBC vs non-TNBC: a retrospective review of differences in mean age, family history, smoking history, and stage at diagnosis. *Clin. Adv. Hematol. Oncol.* **12**, 377–381
13. Schimmel, J., Eifler, K., Sigurethsson, J. O., Cuijpers, S. A., Hendriks, I. A., Verlaan-de Vries, M., *et al.* (2014) Uncovering SUMOylation dynamics during cell-cycle progression reveals FoxM1 as a key mitotic SUMO target protein. *Mol. Cell* **53**, 1053–1066
14. Seo, J. S., Kim, H. N., Kim, S. J., Bang, J., Kim, E. A., Sung, K. S., *et al.* (2014) Cell cycle-dependent SUMO-1 conjugation to nuclear mitotic apparatus protein (NuMA). *Biochem. Biophys. Res. Commun.* **443**, 259–265
15. Kumar, A., and Zhang, K. Y. (2015) Advances in the development of SUMO specific protease (SENP) inhibitors. *Comput. Struct. Biotechnol. J.* **13**, 204–211
16. Mukhopadhyay, D., and Dasso, M. (2007) Modification in reverse: the SUMO proteases. *Trends Biochem. Sci.* **32**, 286–295
17. Hickey, C. M., Wilson, N. R., and Hochstrasser, M. (2012) Function and regulation of SUMO proteases. *Nat. Rev. Mol. Cell Biol.* **13**, 755–766
18. Teschke, R., Frenzel, C., Glass, X., Schulze, J., and Eickhoff, A. (2012) Greater Celandine hepatotoxicity: a clinical review. *Ann. Hepatol.* **11**, 838–848
19. Zhang, Y., Yang, K., Yang, J., Lao, Y., Deng, L., Deng, G., *et al.* (2020) SENP3 suppresses osteoclastogenesis by De-conjugating SUMO2/3 from IRF8 in bone marrow-derived monocytes. *Cell Rep.* **30**, 1951–1963.e4
20. Liu, K., Guo, C., Lao, Y., Yang, J., Chen, F., Zhao, Y., *et al.* (2020) A fine-tuning mechanism underlying self-control for autophagy: deSUMOylation of BECN1 by SENP3. *Autophagy* **16**, 975–990
21. Li, K., Deng, Y., Deng, G., Chen, P., Wang, Y., Wu, H., *et al.* (2020) High cholesterol induces apoptosis and autophagy through the ROS-activated AKT/FOXO1 pathway in tendon-derived stem cells. *Stem. Cell Res. Ther.* **11**, 131
22. Yang, B., Ding, L., Chen, Y., and Shi, J. (2020) Augmenting tumor-starvation therapy by cancer cell autophagy inhibition. *Adv. Sci. (Weinh)* **7**, 1902847
23. Zhou, Z., Wang, M., Li, J., Xiao, M., Chin, Y. E., Cheng, J., *et al.* (2016) SUMOylation and SENP3 regulate STAT3 activation in head and neck cancer. *Oncogene* **35**, 5826–5838
24. Xiao, M., Bian, Q., Lao, Y., Yi, J., Sun, X., Sun, X., *et al.* (2022) SENP3 loss promotes M2 macrophage polarization and breast cancer progression. *Mol. Oncol.* **16**, 1026–1044
25. Zhu, Y. Z., Zhang, J. S., Yu, L. F., Xu, S. W., Chen, L., Wu, K. L., *et al.* (2023) SENP3 promotes tumor progression and is a novel prognostic biomarker in triple-negative breast cancer. *Front. Oncol.* **12**, 972969
26. Moroishi, T., Park, H. W., Qin, B., Chen, Q., Meng, Z., Plouffe, S. W., *et al.* (2015) A YAP/TAZ-induced feedback mechanism regulates Hippo pathway homeostasis. *Genes Dev.* **29**, 1271–1284
27. Ji, L., Li, X., Zhou, Z., Zheng, Z., Jin, L., and Jiang, F. (2020) LINC01413/hnRNP-K/ZEB1 Axis accelerates cell proliferation and EMT in colorectal cancer via inducing YAP1/TAZ1 translocation. *Mol. Ther. Nucleic Acids* **19**, 546–561
28. Wang, Z., Kong, Q., Su, P., Duan, M., Xue, M., Li, X., *et al.* (2020) Regulation of Hippo signaling and triple negative breast cancer progression by an ubiquitin ligase RNF187. *Oncogenesis* **9**, 36
29. Deng, Q., Jiang, G., Wu, Y., Li, J., Liang, W., Chen, L., *et al.* (2018) GPER/Hippo-YAP signal is involved in Bisphenol S induced migration of triple negative breast cancer (TNBC) cells. *J. Hazard Mater.* **355**, 1–9
30. Vici, P., Ercolani, C., Di Benedetto, A., Pizzuti, L., Di Lauro, L., Sperati, F., *et al.* (2016) Topographic expression of the Hippo transducers TAZ and YAP in triple-negative breast cancer treated with neoadjuvant chemotherapy. *J. Exp. Clin. Cancer Res.* **35**, 62
31. Yan, F., Qian, M., He, Q., Zhu, H., and Yang, B. (2020) The post-translational modifications of Hippo-YAP pathway in cancer. *Biochim. Biophys. Acta Gen. Subj.* **1864**, 129397
32. Zhang, Z., Du, J., Wang, S., Shao, L., Jin, K., Li, F., *et al.* (2019) OTUB2 promotes cancer metastasis via hippo-independent activation of YAP and TAZ. *Mol. Cell* **73**, 7–21.e7
33. Kakarala, M., and Wicha, M. S. (2008) Implications of the cancer stem-cell hypothesis for breast cancer prevention and therapy. *J. Clin. Oncol.* **26**, 2813–2820
34. Burstein, S. M. (2008) Daily life in ancient Egypt: recreating Lahun. *Choice: Curr. Rev. Acad. Lib.* **46**, 754
35. Zou, H., Luo, J., Guo, Y., Liu, Y., Wang, Y., Deng, L., *et al.* (2022) RNA-binding protein complex LIN28/MSI2 enhances cancer stem cell-like properties by modulating Hippo-YAP1 signaling and independently of Let-7. *Oncogene* **41**, 1657–1672
36. Chang, H. M., and Yeh, E. T. H. (2020) SUMO: from bench to bedside. *Physiol. Rev.* **100**, 1599–1619
37. Chen, X., Qin, Y., Zhang, Y., Yang, X., Xing, Z., Shen, Y., *et al.* (2022) SENP2-PLCbeta4 signaling regulates neurogenesis through the maintenance of calcium homeostasis. *Cell Death Differ.* **29**, 337–350
38. Hu, Z., Teng, X. L., Zhang, T., Yu, X., Ding, R., Yi, J., *et al.* (2021) SENP3 senses oxidative stress to facilitate STING-dependent dendritic cell antitumor function. *Mol. Cell* **81**, 940–952.e5
39. Tong, Y. Y., Zhang, Z., Cheng, Y. R., Yang, J., Fan, C., Zhang, X. Y., *et al.* (2022) Hypoxia-induced NFATc3 deSUMOylation enhances pancreatic carcinoma progression. *Cell Death Dis.* **13**, 413
40. Ma, S., Wu, Z., Yang, F., Zhang, J., Johnson, R. L., Rosenfeld, M. G., *et al.* (2021) Hippo signalling maintains ER expression and ER(+) breast cancer growth. *Nature* **591**, E1–E10
41. Shen, J., Cao, B., Wang, Y., Ma, C., Zeng, Z., Liu, L., *et al.* (2018) Hippo component YAP promotes focal adhesion and tumour aggressiveness via transcriptionally activating THBS1/FAK signalling in breast cancer. *J. Exp. Clin. Cancer Res.* **37**, 175
42. Xu, J., Fang, X., Long, L., Wang, S., Qian, S., and Lyu, J. (2021) HMGA2 promotes breast cancer metastasis by modulating Hippo-YAP signaling pathway. *Cancer Biol. Ther.* **22**, 5–11
43. Lapi, E., Di Agostino, S., Donzelli, S., Gal, H., Domany, E., Rechavi, G., *et al.* (2008) PML, YAP, and p73 are components of a proapoptotic autoregulatory feedback loop. *Mol. Cell* **32**, 803–814
44. Ma, S., Meng, Z., Chen, R., and Guan, K. L. (2019) The Hippo pathway: biology and pathophysiology. *Annu. Rev. Biochem.* **88**, 577–604